Electronic states, ionization potentials, and bond energies of TlH n , InH n , TlH+ n , and InH+ n (n=1–3)

K. Balasubramanian and J. X. Tao

Citation: The Journal of Chemical Physics **94**, 3000 (1991); doi: 10.1063/1.459823
View online: http://dx.doi.org/10.1063/1.459823
View Table of Contents: http://scitation.aip.org/content/aip/journal/jcp/94/4?ver=pdfcov
Published by the AIP Publishing

Electronic states, ionization potentials, and bond energies of TlH_n, InH_n, TlH_n^+, and InH_n^+ ($n=1$–3)

K. Balasubramanian[a] and J. X. Tao
Department of Chemistry, Arizona State University, Tempe, Arizona 85287-1604

(Received 31 July 1990; accepted 16 November 1990)

Potential energy surfaces of 6 electronic states of TlH_2 and InH_2 and 8 electronic states of TlH_2^+ and InH_2^+ are computed. In addition the ground states of TlH_3, InH_3, TlH_3^+, InH_3^+, TlH, and TlH^+ are investigated. A complete active space multiconfiguration self-consistent field (CAS-MCSCF) followed by second-order configuration interaction (SOCI) and relativistic configuration interaction (RCI) including spin–orbit coupling calculations are carried out. The step-wise bond energies, $D_e(H_{n-1}M\text{–}H)$ and adiabatic ionization potentials are computed. The ground states of TlH_2 and InH_2 are found to be bent ($^2A_1$; $\theta_e \sim 121.5°$, 120°) while the ground states of TlH_2^+ and InH_2^+ are linear ($^1\Sigma_g^+$). The ground states of TlH_3 and InH_3 are found to be $^1A_1$ (D_{3h}) states while the ground states of TlH_3^+ and InH_3^+ are Jahn–Teller distorted $^2B_2(C_{2v})$ states. The unique bond length of TlH_3^+ and InH_3^+ is shorter than the two equal bond lengths. The bond angles (H–M–H) for TlH_3^+ and InH_3^+ deviate considerably from the neutral $\theta_e = 120°$ to near 69°. The TlH^+ ion is found to be only 0.04 eV stable. Periodic trends in the geometries, bond energies and IPs are studied. Spin–orbit effects were found to be significant for TlH_n species. The IPs of InH_n and TlH_n exhibit odd–even alternation. The bond energies also show an interesting trend as a function of n.

I. INTRODUCTION

Experimental and theoretical studies of Group (III), Group (IV), and Group (V) hydride clusters and related methyls are on the increase in recent years.[1–36] Many of these hydrides are sources for the corresponding elements to generate semi-conductor layers comprising these elements in chemical vapor deposition (CVD). The bond energies, ionization potentials, and appearance potentials of hydrides such as BH_n, AsH_n, PH_n, SiH_n, etc., have been the topic of several experimental and theoretical studies. The related trimethyl gallium [$Ga(CH_3)_3$] and trimethyl indium [$In(CH_3)_3$] have been studied since these are used in the development of microelectronic devices.[25]

Berkowitz and co-workers[23,24,26,30] have used the photoionization method to study the ionization potentials and appearance potentials of hydrides such as BH_n, AsH_n, PH_n, SiH_n, and GeH_n. The stepwise bond energies and energy separations of the low-lying states can be deduced from such experiments. The determination of the excited state energy separations and bond energies could be difficult since the appearance potentials cannot often be exactly obtained. Theoretical calculations could be quite valuable for the elucidation of the low-lying electronic states and the computation of bond energies and adiabatic ionization potentials.

While lighter hydride clusters such as BH_n, SiH_n, GeH_n, etc.,[16–28] have been extensively studied there is very little information available on heavier hydride clusters such as InH_n and TlH_n. Theoretical studies of such species are scarce due to the large number of electrons, relativistic effects, and the possibility of several low-lying electronic states.

Among very heavy hydrides, the thallium hydride (TlH) has been studied theoretically very extensively as this presents an interesting case to test relativistic quantum mechanical techniques. Pitzer and co-workers[1,3] used a simple SCF procedure within the ω-ω coupling scheme to study TlH. Subsequently, there have been several sophisticated relativistic calculations including the relativistic configuration interaction method[9] which includes spin–orbit coupling and electron correlation effects simultaneously.

There appears to be no theoretical studies at present on TlH_2, TlH_2^+, InH_2, InH_3, InH_2^+, InH_3^+, and TlH_3^+. The TlH_3 molecule has been studied in the ground state using a quasi
relativistic and nonrelativistic approaches.[10] However, the stepwise bond energy for all these species has not been obtained and the level of theory employed here is superior to the previous methods.

The objective of this study is to carry out complete active space MCSCF/second-order CI (SOCI)/relativistic CI (RCI) calculations on TlH, TlH^+, TlH_2, TlH_2^+, InH_2, InH_2^+, TlH_3, InH_3, TlH_3^+, and InH_3^+. We compute the entire bending potential energy surfaces of 6 electronic states of TlH_2, InH_2 and 8 electronic states of TlH_2^+ and InH_2^+. The adiabatic ionization potentials, equilibrium geometries, stepwise bond energies, and dipole moments of all these species are computed and compared with available data on BH_n and GaH_n. It is shown that TlH_n species behave differently due to relativistic effects. The spin–orbit contaminations of other states even at the ground state geometries of TlH_n are shown to be non-negligible. This manifests strongly in the case of TlH_2 by changing its equilibrium bond angle. Section II describes our method of calculations while Sec. III comprises results and discussions. Section IV consists of the analyses of electronic states while Sec. V investigates the size dependencies of IPs and bond energies. Section VI consists

[a] Camille and Henry Dreyfus Teacher-Scholar.

 0021-9606/91/043000-11$03.00

of a critical comparison of our results with lighter Group III analogs with the objective of enlightening periodic trends.

II. METHOD OF COMPUTATIONS

Relativistic effective core potentials (RECPs) which retained the outer $(n-1)\,d^{10}ns^2np^1$ shells of In and Tl, in the valence space were used uniformly in all studies here. We employ the RECPs generated by Ross *et al.*[37] for Tl and by La John *et al.*[38] for In, respectively. We start with the valence Gaussian $(3s3p3d)$ Gaussian basis set for Tl and In atom. The two large d exponent functions corresponding to the $(n-1)d^{10}$ shells were contracted. To this basis set an additional set of diffuse d functions to polarize the outer np shells were added. The resulting basis set is of $(3s3p4d/3s3p3d)$ quality for Tl. For the In atom we employed a more extended $(4s4p4d/4s4p3d)$ basis set. For the hydrogen atoms we uniformly used the van Duijneveldt $(5s1p/3s1p)$ basis set.[39]

A complete active space MCSCF (CAS-MCSCF) method was used to generate the orbitals for higher second-order CI (SOCI) calculations. The CAS-MCSCF calculations were performed in the full CI space obtained by distributing the valence ns^2np^1 shells of In and Tl and the $1s^1$ shell of the hydrogen atoms in all possible ways among a chosen set of orbitals referred to as the active space. The active space for all TlH_n and InH_n calculations consisted of the outer ns, all three np orbitals of the metal atom and the $1s$ orbitals of the hydrogen atoms. The $(n-1)d^{10}$ shells were allowed to relax but no excitations from these orbitals were allowed at the CAS-MCSCF stage. The CAS-MCSCF calculations of the positive ions included one electron less than the neutral species.

The second-order CI(SOCI) calculations included (i) all configurations in the CAS-MCSCF, (ii) those configurations obtained by distributing N_v-1 electrons (N_v = No. of active electrons) in all possible ways among the CAS-MCSCF internal space of orbitals and 1 electron in the external space in all possible ways, (iii) all configurations obtained by distributing N_v-2 electrons in the internal space, and 2 electrons in the external space in all possible ways. The SOCI calculations included up to 91 400 CSFs. We also estimated the effect of unlinked quadruple clusters using the Davidson correction method to the SOCI wave function. In general, the Davidson correction had very little impact on the SOCI r_e. The bond lengths changed by 0.001 Å or less. Even the total energy lowered by less than a millihartree due to Davidson's correction. Consequently, the SOCI wave function appears to be satisfactory for the properties that we compute in this study.

We optimized the geometries using a multidimensional quadratic fit near the minimum. The geometries obtained using nonanalytical gradient methods tend to be a bit less accurate compared to the gradient methods but we used a small enough grid (± 0.05 Å) for the final fit to ensure that the errors are minimized. The dissociation energies reported in this study are D_e values and thus we have not subtracted the zero-point energies from the computed D_e values.

In all CASSCF and SOCI calculations the $(n-1)d^{10}$ shells were kept in core. At the CASSCF stage there exits a possibility that the d orbitals can rotate to the active space leading to errors in correlation energies. In all calculations described here, however, the d orbitals were always in the inactive space. This was accomplished by starting with an appropriate set of input orbitals by first freezing the d and subsequently allowing the d shells to relax. Once a satisfactory set of orbitals were obtained for the first geometry all subsequent points were obtained using the converged set of orbitals obtained for the starting geometry. This technique prevented the possibility of rotation of the d orbitals into the active space.

The effect of spin–orbit coupling was introduced using the relativistic configuration interaction (RCI) method. The spin–orbit integrals obtained using Pitzer's codes[40] were transformed in the SOCI natural orbital basis. The transformed integrals were added to the appropriate one-electron CI Hamiltonian matrix elements in the RCI. The RCI calculations, in general, included all those configurations with the same symmetry in the spin–double group of the molecular symmetry group. For example, the RCI calculations on the $^2A_1$ state of TlH_2 included, the $^2A_1$ configuration with open shell spin α, the $^2B_1$ state with spin β, the $^2B_2$ state with spin β, and a low-lying $^4A_2$ with spin CSF combinations $\alpha\beta\alpha$, $\alpha\alpha\beta$, $\beta\alpha\alpha$, and $\beta\beta\beta$. The RCI calculations of TlH_3 included in the C_{2v}^2 symmetry $^1A_1(A_1)$, $^3B_1(A_1)$, $^3B_2(A_1)$, and $^3A_2(A_1)$ states, where labels inside the parentheses correspond to the overall symmetry in the C_{2v}^2 group. In Refs. 41 and 42, appropriate symmetry-adapted spin combinations have been worked out for triplet spin functions.

The accuracy of our CASSCF/SOCI/RCI method and the basis set was gauged by comparing our computed results with the known atomic $Tl(^2P_{1/2})$–$Tl(^2P_{3/2})$ separation.[43] We made CASSCF/SOCI/RCI calculations of the $2(I)$ state and the $0^+(I)$ state of TlH at 8.0 Å using the same basis set. Since the $2(I)$ and 0^+ states of TlH correlate into $Tl(^2P_{3/2})$ and $Tl(^2P_{1/2})$, respectively, the computed splitting at 8.0 Å measures the atomic $Tl(^2P_{3/2})$–$Tl(^2P_{1/2})$ splitting. Our CASSCF/SOCI/RCI splitting of 6930 cm^{-1} compares very well with an experimental value of 7800 cm^{-1} and a previous theoretical value of 7400 cm^{-1} obtained by Christiansen *et al.*[9] for the Tl atom using a STO basis set.

Our CASSCF/SOCI $In(^2P)$–$In(6s;^2S)$ and $In(^2P)$–$In(6p;^2P)$ separations are 22 500 and 30 170 cm^{-1} compared to the experimental values of 24 370 and 31 817 cm^{-1}, respectively. Consequently, the basis sets employed are of adequate flexibility not only for the valence states but also some low-lying Rydberg states of In and Tl atoms.

All CASSCF/SOCI calculations described here were made using one of the author's[41] modified versions of ALCHEMY codes.[44] The RCI calculations were carried out using the RCI method for polyatomics described in Ref. 33.

III. RESULTS AND DISCUSSIONS

A. TlH_2

1. Potential energy surfaces and equilibrium geometries

Figure 1 shows the bending potential energy surfaces of 4 electronic states of TlH_2 obtained at the CAS-MCSCF lev-

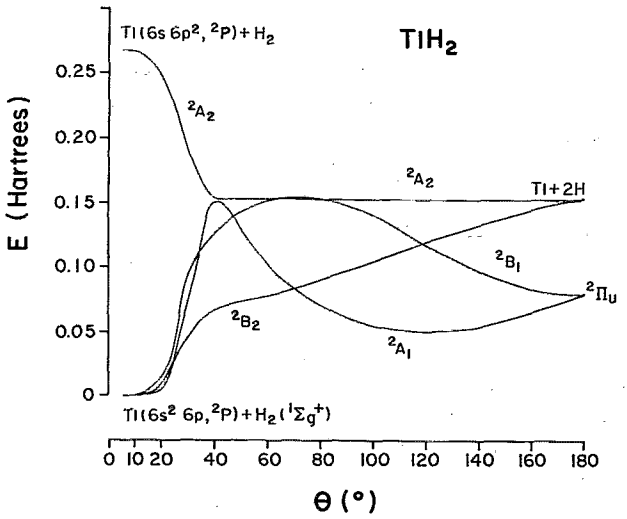

FIG. 1. Bending potential energy surfaces of TlH_2.

el. As seen from this figure, the ground state of TlH_2 is a $^2A_1$ electronic state with a relatively shallow surface in the obtuse angle region. The $^2A_1$ state arises from the $Tl(6s^26p)^2P + H_2$ species. It has a sharp barrier and an obtuse minimum near $\theta \sim 1$ which corresponds to a sp^2 hybridization.

The $^2B_1$ state arising also from $Tl(^2P) + H_2$ forms a broad barrier and then a linear minimum coinciding with the $^2A_1$ linear saddle point. The $^2B_2$ state to the contrary is predominantly repulsive and dissociative as seen from Fig. 1. In the linear limit this state actually dissociates into $Tl(^2P) + H + H$.

The $^2A_2$ arises from the $Tl(6s6p^2,^2D) + H_2$ species. In this state the Tl atom dissociates H_2 but its energy is so high that it forms the dissociated Tl + H + H and no stable TlH_2 bent minimum can be found in the $^2A_2$ state.

The crossing of $^2A_1$ and $^2B_2$ bending surfaces is interesting but the bond lengths are sufficiently different at this θ so that this does not correspond to the crossing of the global potential energy surfaces.

The spin–orbit contamination of the $^2A_1$ and $^2B_2$ states near the bending PES crossing (as well as the $^2A_1$ and $^2B_1$ mixing) and at obtuse bond angles is expected to be non-negligible. This will be discussed later.

Table I shows the actual CASSCF and SOCI equilibrium geometries of the electronic states of TlH_2. As evidenced from this table, the ground state of TlH_2 is a $^2A_1$ state with $r_e = 1.85$ Å and $\theta_e = 121.5°$. It is 1.36 eV unstable relative to $Tl(^2P) + H_2$ but is considerably more stable than TlH + H as we will discuss.

The $^2A_1$ and $^2B_1$ states correlate into $^2\Pi_u$ in the linear limit which is 0.77 eV above the bent $^2A_1$ minimum. It is comforting that the difference in the CASSCF and SOCI energy separations is not substantial. The r_e of the $^2A_1$ state, however, decreases by 0.02 Å at the SOCI level.

The dipole moment of the $^2A_1$ state of TlH_2 at its equilibrium geometry is 0.23 D with the Tl^+H^- polarity. This is consistent with the electro-positive character of the Tl atom.

2. Spin–orbit effects

The ground state $^2P_{1/2}$–$^2P_{3/2}$ experimental energy separation[43] of Tl is 7800 cm^{-1} compared to our value of 6900 cm^{-1}. Hence, the spin–orbit effects could be important. However, in the molecular region of the potential energy surfaces in general, spin–orbit effects are not as significant as the atomic splitting. This is especially so for the closed-shell species such as TlH and TlH_3. It would be interesting to study the effect of SO coupling both on energy separations and in the mixing with other electronic states.

Table II shows the effect of spin–orbit coupling on both TlH_2 and other species. The spin–orbit coupling stabilizes the $^2A_1$ state of TlH_2 by 0.112 eV while the atomic $^2P_{1/2}$–$^2P_{3/2}$ splitting is much more substantial ($\sim$7800 cm^{-1}).[43] Consequently, the SO coupling is small for TlH_2 but non-negligible. Since the spin–orbit correction is small near the well but large at the $Tl + H_2$ dissociation limit, it destablilizes TlH_2 relative to $Tl + H_2$ by 0.4 eV and hence the final energy separation of the E state of TlH_2 with respect to $Tl(^2P_{1/2}) + H_2$ is 1.76 eV higher. Therefore, TlH_2 is considerably unstable relative to $Tl(^2P_{1/2}) + H_2$.

The spin–orbit coupling also contaminates the $^2A_1$ state of TlH_2 especially, with the low-lying excited $^2B_1$ state near the well of the $^2A_1$ state. At the linear limit, of course, these states become degenerate $^2\Pi_u$. The spin–orbit coupling splits this state into the $(1/2)_u$ and $(3/2)_u$ components. The $(1/2)_u$ component will be lower since the $^2\Pi_u$ state arises from a $1\sigma_g^2 1\sigma_u^2 1\pi_u$ electronic configuration. However, the SO splitting even in the linear limit of the ground state is smaller than the atomic splitting. For the $^2A_2$, $^4A_2$, and $^2B_2$ states, however, in the linear limit the spin–orbit effects are substantial since they dissociate into Tl + H + H.

TABLE I. The geometries and energy separations of the two lowest electronic states of TlH_2.

State	CASSCF R_e(Å)	CASSCF θ_e(°)	CASSCF E^a(eV)	SOCI R_e(Å)	SOCI θ_e(°)	SOCI E^b(eV)	SOCI μ_e(D)
$^2A_1$	1.869	121.1	1.347	1.854	121.5	1.362	0.230
$^2\Pi_u$	1.732	180.0	2.149	1.723	180.0	2.135	

[a] Zero energy for the CASSCF is for $Tl(6s^26p,^2P) + H_2 = -51.242\,878$ hartrees.
[b] Zero energy for the SOCI is for $Tl(6s^26p,^2P) + H_2 = -51.273\,7198$ hartrees.

TABLE II. Equilibrium geometries and energy separations including spin–orbit effects for TlH_2, InH_2, TlH_2^+, and InH_2^+.

State	Molecule	R_e(Å)	θ_e(°)	E(eV)[a]
$^2A_1(E)$	InH_2	1.782	119.7	0.513
$^2A_1(E)$	TlH_2	1.844	122.4	1.247
$^1A_1(A_1)$	InH_2^+	1.696	180	1.651
$^1A_1(A_1)$	TlH_2^+	1.726	180	2.388

[a] With respect to $M + H_2$ and $M^+ + H_2$ ground states.

3. Bond energies

The CAS-MCSCF/SOCI/RCI calculations of TlH were also carried out with the objective of computing the bond energies. For TlH our spin–orbit corrected D_e of 48 kcal/mole is slightly improved compared to the previous reported value by Christiansen *et al.*[9] The present value is in excellent agreement with the experimental value of 47.6 kcal/mole.

The D_e(HTl–H) was deduced from the spin–orbit corrected SOCI energies of TlH_2 and TlH + H. The value obtained this way is 21.4 kcal/mole. This evidently suggests that D_e(HTl–H) is significantly smaller than D_e(Tl–H), consistent with the somewhat unstable nature of TlH_2 relative to $Tl + H_2$. We expect our spin–orbit-corrected SOCI bond energy to be accurate to $\pm$ 3 kcal/mole.

B. InH_2

1. Potential energy surfaces and equilibrium geometries

Figure 2 shows the bending potential energy surfaces of six electronic states of InH_2. The potential energy surfaces of InH_2 are qualitatively similar to the corresponding states of TlH_2. For InH_2 we studied the PES of two more electronic states. The ground state of InH_2 is unambiguously a $^2A_1$ state. The actual equilibrium geometries at both CAS-MCSCF and SOCI levels of theories are shown in Table III.

The $^2A_1$ ground state of InH_2 has an equilibrium θ_e of 119.7° and R_e = 1.782 Å at the highest level of theory. The

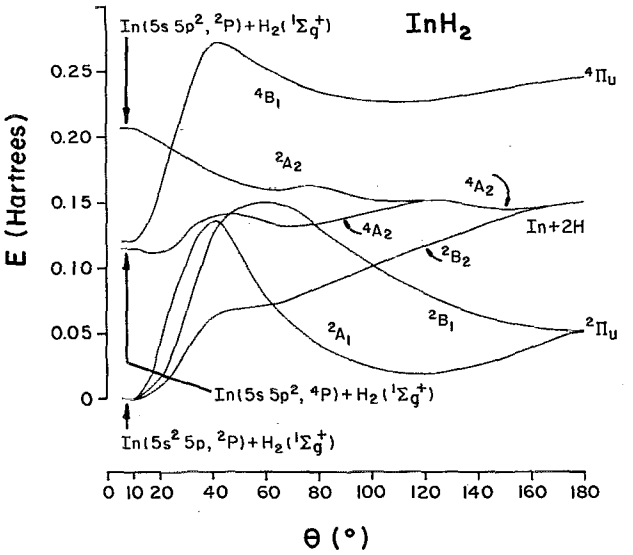

FIG. 2. Bending potential energy surfaces of InH_2.

In–H bond lengths in InH_2 are expected to be shorter compared to the diatomic InH for which the experimental r_e is well established at 1.838 Å.[45] The shorter In–H bond length in InH_2 compared to InH is quite similar to the bond lengths in TlH_2 and TlH molecules.

The InH_2 ($^2A_1$) ground state is 0.52 eV less stable compared to In(^2P) + H_2. Hence InH_2 is more stable than TlH_2 with respect to the dissociation limit but less stable compared to GaH_2. The analogous $^2A_1$ ground state of GaH_2 is nearly degenerate (0.04 eV above) with respect to Ga(^2P) + H_2 dissociated species. The linear $^2\Pi_u$ state is 1.32 eV higher than the bent minimum for InH_2 while the corresponding separations for GaH_2 and TlH_2 are 1.11 eV (Ref. 21) and 2.14 eV, respectively.

As seen from Fig. 2, the $^4A_2$, $^2B_2$, and $^2A_2$ states of InH_2 are dissociative in that they do not form stable molecules and dissociate into In + H + H at the linear limit. Analogous to TlH_2, the $^2A_1$ state of InH_2 has a sharp barrier due to an avoided crossing while the $^2B_1$ surface has a somewhat broader barrier. The $^2A_1$ and $^2B_2$ bending surfaces of InH_2 also cross similar to TlH_2. The spin–orbit effects were found

TABLE III. Geometries and energy separations of electronic states of InH_2.

	CASSCF			SOCI			
State	R_e(Å)	θ_e(°)	E[a] (eV)	R_e(Å)	θ_e(°)	E[b] (eV)	μ_e(D)
$^2A_1$	1.802	118.9	0.577	1.782	119.7	0.523	0.211
$^2A_2$	1.976	65.8	4.356				
$^4B_1$	2.128	109.8	6.182				

	Linear states			
State	R(Å)	E[a] (eV)	R(Å)	E[b] (eV)
$^2\Pi_u$	1.714	1.422	1.701	1.320
In + 2H	···	4.148	···	4.483
$^4\Pi_u$	2.370	6.684		

[a] Zero energy for the CASSCF is for In($5s^25p\ ^2P$) + H_2 = − 57.820 663 hartrees.
[b] Zero energy for the SOCI is for In($5s^25p\ ^2P$) + H_2 = − 57.852 905 hartrees.

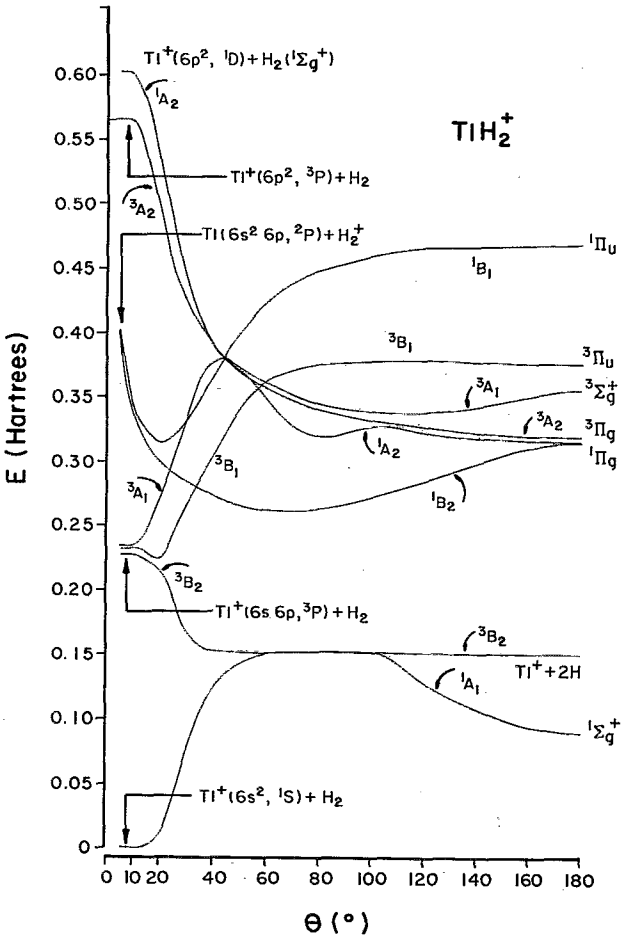

FIG. 3. Bending potential energy surfaces of TlH_2^+.

to be significantly smaller for InH_2 and hence we do not discuss these effects in detail.

2. Bond energies

The CAS-MCSCF/SOCI/RCI calculations of the diatomic InH in the $X\,{}^1\Sigma^+$ ground state were also made with the objective of comparing the bond energy, D_e(HIn–H). The calculated D_e (In–H) is 2.58 eV in excellent agreement with an experimental value of 2.57 eV.[46] We deduce from the SOCI energies of InH and InH_2, the D_e (HIn–H) as 31.5 kcal/mole. The D_e (HGa–H) obtained in a previous study is 41 kcal/mole. Hence the In–H bond in InH_2 is weaker compared to GaH_2. This is also consistent with the fact that theoretical D_e (GaH) = 2.81 eV (Ref. 21) compared to an experimental value of 2.80 eV.[45]

C. TlH_2^+

Figure 3 shows the potential energy surfaces for eight electronic states of TlH_2^+. The ground state of Tl^+ is a ^1S state arising from the $6s^2$ electronic configuration. It is not expected to be strongly reactive due to its closed shell character. As seen from Fig. 3, this state of Tl^+ forms a linear TlH_2^+ ion in the $^1\Sigma_g^+$ state.

The excited ^3P state of Tl^+ is more reactive as seen from Fig. 3. The first state readily dissociates H_2 but it dissociates into $Tl^+(^3P) + H(^2S) + H(^2S)$. Hence the surface is completely flat for $\theta > 40°$. Consequently, the merging of the $^1A_1$ surface of TlH_2^+ with this surface in this region is clearly suggestive of the formation of $Tl^+ + H(^2S) + H(^2S)$. However, the energy required to excite the system to this region is almost the D_e of H_2.

The excited $Tl^+(6s6p,{}^3P)$ ion also forms a weak complex in the $^3B_1$ state. But the $^3A_1$ state has to surmount a large barrier prior to insertion into H_2.

It is interesting to note that the $^1B_2$ and $^1B_1$ states of TlH_2^+ arise from $Tl(^2P) + H_2^+$ in contrast with the corresponding states of InH_2^+ which arise from $In^+(5s5p,{}^1P) + H_2$. This is primarily due to the fact that $Tl^+(^1P)$ is much higher in energy. Furthermore, the spin–orbit coupling of the $^3P_1$ with $^1P_1$ components will evidently raise the $^1P_1$ state of Tl^+ further. As seen from Fig. 3, the $^3B_1$ and $^3A_1$ curves of TlH_2^+ cross the $^1B_2$ curve. We expect considerable charge transfer in this region.

As seen from Fig. 3, the ^3P and ^1D states of the Tl^+ ion at least in the $^3A_2$ and $^1A_2$ channels are very reactive. Consequently, the potential energy surfaces of TlH_2^+ reveal an interesting trend, viz., the excited states of the ion are far more reactive than the closed shell ground state of the ion.

Table IV shows the equilibrium geometries of the ground state and an excited $^1\Pi_g$ state. The ground state of TlH_2^+ ($^1\Sigma_g^+$) has an $r_e = 1.73$ Å. It is 2.44 eV unstable relative to $Tl^+ + H_2$. This is not surprising since we do not expect TlH^+ to be very stable relative to $Tl^+ + H$ (see Sec. IIIG.). However, TlH_2^+ is stable relative to $TlH^+ + H$ by 2.2 eV or equivalently the bond energy, $D_e(HTl^+ - H)$ is 2.2 eV. The TlH_2^+ ion is the most stable of the TlH_n^+ cluster ions.

A critical comparison of the ground state geometry of the neutral TlH_2 and TlH_2^+ reveals that the r_e shrinks upon ionization by almost 0.05 Å. The bond angle changes from a neutral $\theta_e = 119.7°$ to a linear geometry for the ion. Therefore, the Franck–Condon factor for the photoelectron spectral transition $TlH_2(^2A_1) \rightarrow TlH_2^+(^1\Sigma_g^+) + e^-$ should be small. It is also worth noting that upon inclusion of spin–orbit effects, the stabilities of TlH_2 and TlH_2^+ relative to $Tl(^2P) + H_2$ and $Tl^+(^1S) + H_2$ become comparable.

The adiabatic ionization potential of $TlH_2(^2A_1)$ to form

TABLE IV. Geometries and energy separations of electronic states of TlH_2^+.

	CASSCF		SOCI	
		Linear states		
State	R_e(Å)	E^a (eV)	R(Å)	E^b (eV)
$^1\Sigma_g^+$	1.744	2.454	1.729	2.441
$^1\Pi_g$	1.915	8.59		
$^3\Pi_g$	1.88	8.71		
$^3\Pi_u$	2.33	10.26		

[a] Zero energy for the CASSCF is for $Tl^+(6s^2,{}^1S) + H_2 = -51.068\,466$ hartrees.

[b] Zero energy for the SOCI is for $Tl^+(6s^2,{}^1S) + H_2 = -51.086\,521$ hartrees.

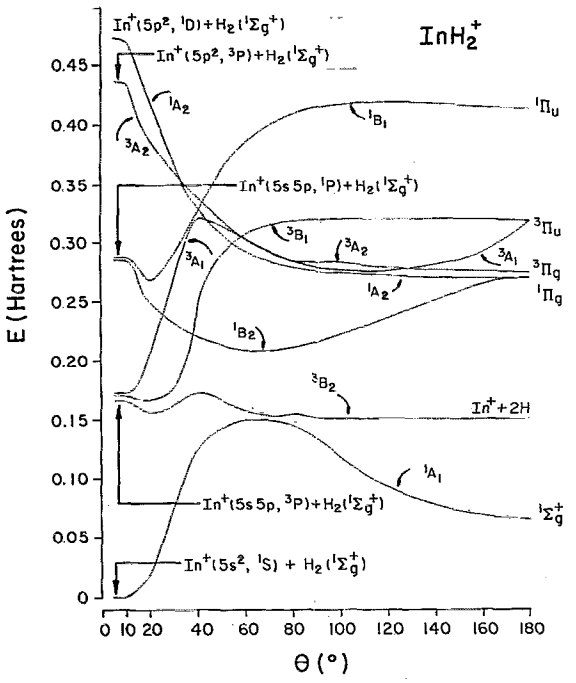

FIG. 4. Bending potential energy surfaces of InH_2^+.

the TlH_2^+ ($^1\Sigma_g^+$) ground state including the spin–orbit effects is calculated as 6.23 eV at the highest SOCI/RCI level of theory. We expect the IP to decrease as one goes down the periodic table.

D. InH_2^+

Figure 4 shows the bending potential energy surfaces of InH_2^+ while Table V shows the actual geometries and energy separations. The InH_2^+ ion has several qualitative similarities to TlH_2^+. The ground state of InH_2^+ is also a linear $^1\Sigma_g^+$ state arising from $In^+(5s^2,{}^1S) + H_2$. The In^+ (^1S) ion does not insert into H_2. The barrier that ground state ion has to surmount is almost equal to the D_e of H_2.

The excited $In^+(5s5p,{}^3P)$ ion forms a weak complex with H_2 in the $^3B_2$ state and dissociates for $\theta > 50°$ into $In^+ + H(^2S) + H(^2S)$. The other two triplet states have to surmount barriers prior to the formation of the linear $(H–In–H)^+$ molecule. Note that among the states we studied, only $^1B_2$ and $^3A_1$ form bent minima.

The $In^+(5s5p,{}^1P)$ ion inserts spontaneously into H_2 in the $^1B_2$ channel. But in the $^1B_1$ channel it is quite unreactive. The In^+ in the $5p^2$ configuration is also quite reactive analogous to the Tl^+ in the $6p^2$ configuration.

The In–H bond lengths (Table V) of 1.696 Å in InH_2^+ are shorter than the corresponding bond lengths of the neutral InH_2 (1.782 Å). The bond angle of the neutral molecule (119.7°) dramatically contrasts with the InH_2^+ ion which is linear. This means that the Franck–Condon factor for the $InH_2(^2A_1) \rightarrow InH_2^+(^1\Sigma_g^+) + e^-$ will be considerably smaller. All these findings for InH_2^+ are consistent with our calculations of TlH_2^+.

The adiabatic ionization potential of InH_2 including the effects of spin–orbit coupling is calculated as 6.4 eV. We expect the IP of InH_2 to be smaller than InH and InH_3 since ionization of InH_2 results in a closed shell $^1\Sigma_g^+$ ground state, while ionizations of InH and InH_3 destroy the closed shell ground states of these species.

E. TlH_3 and TlH_3^+

1. TlH_3 geometry

The ground state of TlH_3 was found to be a $^1A_1'$ (D_{3h}) state with a planar triangular geometry (Fig. 5). The equilibrium Tl–H bond lengths were found to be 1.791 Å at the SOCI level. The spin–orbit coupling contracts this to 1.788 Å. Our bond length is between the NRPP and QRPP (quasirelativistic) values of 1.837 and 1.745 Å reported by Schwerdtfeger.[10] The relatively shorter Tl–H bond in TlH_3 compared to TlH_2 is primarily attributed to enhanced stability and the ionicities of Tl–H bonds in TlH_3. We expect our Tl–H bond length to be longer than its true value since the same level of (SOCI/RCI) theory yields a r_e of 1.95 Å for TlH compared to an experimental value of 1.87 Å. We be-

TABLE V. Geometries and energy separations of low-lying states of InH_2^+.

	CASSCF			SOCI		
		Linear states				
State	R(Å)	E^a (eV)		R(Å)	E^b (eV)	
$^1\Sigma_g^+$	1.713	1.768		1.696	1.656	
$^1\Pi_g$	1.929	7.356		1.910	7.505	
$^3\Pi_g$	1.904	7.525				
$^3\Pi_u$	2.262	8.672				
$^1\Pi_u$	1.960	11.278				
		Bent states				
State	R_e(Å)	θ_e(°)	E^a (eV)	R_e(Å)	θ_e(°)	E^b (eV)
$^1B_2$	1.877	64.2	5.694	1.861	61.1	5.674
$^3A_1$	2.101	108.8	7.535	2.059	109.9	7.540

[a] Zero energy for the CASSCF is for $In(5s^2,{}^1S) + H_2 = -57.641\,220\,97$ hartrees.
[b] Zero energy for the SOCI is for $In(5s^2,{}^1S) + H_2 = -57.659\,447\,35$ hartrees.

lieve that at least 0.05 Å contraction in the Tl–H bond length is expected from the *d*-core–core and core–valence electron correlation effects. McLean[47] found almost 0.11 Å bond shortening in AgH due to higher-order and inner-shell correlation effects. A similar finding for AuH (Ref. 16) suggests that the *d* electron core–core and core–valence correlation effects for the neighboring TlH_n should be small but non-negligible.

2. Bond energy $D_e(H_2Tl–H)$

The spin–orbit corrected SOCI stepwise bond energy of TlH_3, $D_e(H_2Tl–H)$, is calculated as 60 kcal/mole. The results of bond energies of TlH_n, TlH_n^+, InH_n, and InH_n^+ are summarized in Table VI. This was obtained by comparing the spin–orbit corrected SOCI energies of $TlH_3(^1A_1')$ and $TlH_2(^2A_1)$ + H. Since the bond energy, D_e(HTl-H) is 21.4 kcal/mole while our SOCI/RCI D_e (Tl-H) is 48 kcal/mole, the total bond energy of all bonds in TlH_3 is 129.8 kcal/mole. Our present result is much improved compared to a value of 100.8kcal/mole obtained by Schwerdtfeger[10] using the QRPP method and 115 kcal/mole using the ARPP method. The lower value of Schwerdtfeger is not surprising since the D_e(Tl–H) he obtained are 41.7 and 29 kcal/mole using ARPP and QRPP levels of theory. Since the experimental D_e of Tl–H is established as 47.5 kcal/mole compared to our present value of 48 kcal/mole, we conclude that both the methods used by Schwerdtfeger[10] significantly underestimate the total bond energies of TlH_3 by at least 14 kcal/mole. Our D_e of TlH is 0.5 kcal/mole higher than experiment since the present Gaussian basis set that we use underestimates the spin–orbit splitting of the Tl atom by 900 cm^{-1} compared to the experiment and 500 cm^{-1} compared to the previous STO-RCI calculation.[9] This means the spin–orbit destabilization will be underestimated by 0.9 kcal/mole at the dissociation limit. Hence, our D_e should be corrected by 0.9 kcal/mole or a value of 47.1 kcal/mole obtained for the D_e of TlH in agreement with experiment.

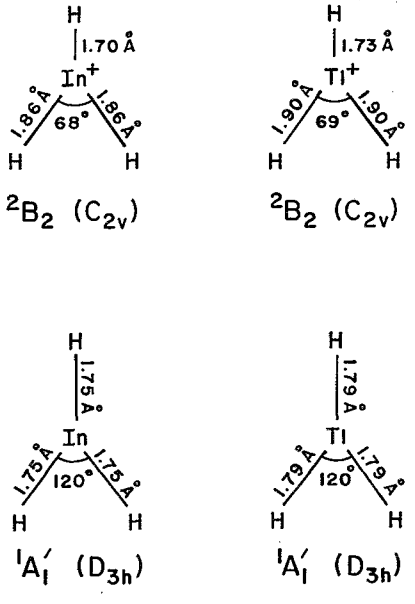

FIG. 5. Equilibrium geometries of TlH_3, TlH_3^+, InH_3, and InH_3^+.

TABLE VI. Bond energies $D_e(H_{n-1}–Tl–H)$, $D_e(H_{n-1}–In–H)$, $D_e(H_{n-1}–Tl^+–H)$, and $D_e(H_{n-1}–In^+–H)$.

Species	D_e (kcal/mole)[a] Theory	Expt
Tl–H	48(47.1)[b]	47.4
TlH^+	0.9	
HTl–H	21.4	
HTl^+–H	51	
H_2Tl–H	60.4	
H_2Tl^+–H	−9.2	
In–H	60	61.4
InH^+	5.3	
HIn–H	31.5	
H_2In–H	70	
H_2In^+–H	−4	

[a] The bond energies include the effect of spin–orbit coupling.
[b] The value in parenthesis is obtained by correcting for the underestimation of the spin–orbit effect (our value 6900 cm^{-1} compared to the experimental value of 7400 cm^{-1}) in our RCI calculations.

3. TlH_3^+ equilibrium geometry

The removal of an electron from the highest occupied orbital of the closed shell $^1A_1'$ ground state of TlH_3 leads to a $^2E'$ state. Consequently, this state undergoes Jahn–Teller distortion leading to $^2B_2$ and $^2A_1$ components in the C_{2v} group. The $^2B_2$ state is the ground state of TlH_3^+. The geometry optimization of TlH_3^+ therefore involved significantly more efforts since three parameters had to be optimized.

In the final optimized structure (Fig. 5), one Tl–H bond contracts (the unique bond) significantly in the $^2B_2$ state to 1.73 Å. The other two equivalent bonds elongate to 1.90 Å. The final H–Tl–H bond angle deviates considerably from the neutral $\theta_e = 120°$ to $\sim 69°$.

The spin–orbit coupling term plays a much more interesting role in TlH_3^+. It couples the two Jahn–Teller components ($^2B_2$ and $^2A_1$) to a non-negligible extent. The mixing of $^2B_2$ with $^2A_1$ was found to be 95% $^2B_2$ and 0.33% $^2A_1$ near the equilibrium geometry of the $^2B_2$ state. The small spin–orbit contamination of the $^2A_1$ state is probably due to a large geometry difference between the $^2B_2$ and $^2A_1$ states.

4. The adiabatic IP of TlH_3 and the stability of TlH_3^+

The adiabatic IP for the ionization process, TlH_3 $(^1A_1') \rightarrow TlH_3^+$ $(^2B_2) + e^-$ including spin–orbit coupling is calculated as 9.24 eV. Note the significant geometry change of the ion compared to the symmetrical neutral TlH_3. Consequently, we expect the Franck–Condon factor for this transition to be smaller. Therefore the photoelectron spectrum of TlH_3 is expected to be broad exhibiting considerable vibrational progression. We find that TlH_3^+ ion is unstable with respect to TlH_2^+ + H by 0.4 eV. This is mainly due to the fact that TlH_2^+ forms a relatively stable closed shell ground state while the neutral TlH_3 forms a stable closed shell ground state.

TABLE VII. RCI composition of electronic states of InH_n and TlH_n.

TlH_2	97% $^2A_1$,	2% $^2B_1$,	0.7% $^4A_2$,	0.15% $^2B_2$
InH_2	99% $^2A_1$,	0.2% $^2B_1$,	0.06% $^4A_2$,	0.01% $^2B_2$
TlH_3	97% $^1A_1'$,	0.5% $^3E''$,	0.1% $^3E'$	
TlH_3^+	95% $^2B_2$,	0.33% $^2A_1$,	0.2% $^4A_1$	
TlH	93% $^1\Sigma^+$,	1.3% $^3\Pi$,	0.5% $^3\Pi$(II)	

F. InH_3 and InH_3^+

1. The equilibrium geometry of InH_3 and bond energies of InH_3

At the highest SOCI level of theory we find InH_3 to be planar–triangular (D_{3h}) (Fig. 5) with a $^1A_1'$ ground state. The In–H bond length at the SOCI level is 1.754 Å. The r_e obtained including the unlinked quadruple clusters using Davidson's correction to the SOCI result is 1.753 Å. We expect the In–H bond lengths in InH_3 to be more accurate than TlH_3 based on good agreement of the calculated r_e of InH with experiment.

As seen from Table VII, the $D_e(H_2In–H)$ obtained using the spin–orbit corrected SOCI level of theory is 70 kcal/mole. Since the D_e(HIn–H) and D_e(In–H) are 31.5 and 60 kcal/mole, the total bond energy of all the bonds in InH_3 is 161.5 kcal/mole. Since our SOCI calculation underestimates the D_e(InH) by 1.4 kcal/mole, we expect the total bond energy to have an error of roughly 5 kcal/mole.

2. Adiabatic IP of InH_3 and the equilibrium geometry of InH_3^+

The InH_3^+ ion has a Jahn–Teller distorted $^2B_2(C_{2v})$ ground state akin to TlH_3^+ and GaH_3^+. At the highest SOCI level of theory the unique In–H bond length is 1.70 Å (Fig. 5). The two equivalent In–H bonds have $r_e = 1.86$ Å. The smaller In–H–In $\theta_e = 68°$, is considerably contracted compared to the neutral $\theta_e = 120°$.

The adiabatic IP of InH_3 for the process $InH_3(^1A';D_{3h}) \rightarrow InH_3^+(^2B_2;C_{2v}) + e$ is calculated as 9.61 eV. The InH_3^+ in the $^2B_2$ state is unstable relative to $InH_2^+(^1\Sigma_g^+) + H(^2S)$ by 4 kcal/mole. Note that the stability of InH_3^+ is considerably reduced compared to the neutral InH_3. This is primarily because the neutral InH_3 is more stable while for the ion, the closed shell $InH_2^+(^1\Sigma_g^+)$ is stabilized.

G. TlH and TlH^+

As noted before, at the highest SOCI/RCI level of theory the $^1\Sigma^+$ ground state of TlH was found to be bound by 48 kcal/mole compared to an experimental D_e of 47.4 kcal/mole. This value is improved compared to the previous value of 41.7 kcal/mole obtained by Christiansen *et al.*[9] and 29 kcal/mole obtained by Schwerdtfeger[10] using the QRPP method. Our best r_e for the $^1\Sigma^+$ ground state of 1.95 Å is improved compared to a value of 1.99 Å obtained by Christiansen *et al.*[9] but is still longer than the experimental r_e of 1.87 Å. We believe that up to 0.005 Å contraction arises from the *d* correlation effects. The remaining of 0.03 Å should be most probably due to basis set limitations and RECPs.

Contrary to Schwerdtfeger,[10] we find TlH^+ to be bound with a $r_e = 3.277$ Å and $D_e = 0.9$ kcal/mole at the highest SOCI/RCI level of theory which included correlation effects to full second order. Schwerdtfeger[10] finds that TlH^+ is unbound at the QRPP level of theory and bound by 0.5 kcal/mole at the ARPP level. But the ARPP method does not include spin–orbit interaction. He obtained r_es of 1.877 and 3.347 Å, using NRPP and ARPP levels of theory and does not list an r_e at the QRPP level presumably because he finds TlH^+ to be unbound at this level. Our bond length is better than his ARPP value of 3.347 Å. Note that our D_e of TlH^+ includes the effect of spin–orbit coupling.

Our adiabatic SOCI/RCI IP of TlH is 7.50 eV. Schwerdtfeger calculates the IP of 6.71 eV using a lower level of theory. It is clear that higher-order correlations effects make significant contributions to the IPs as evidenced by a comparison of the CAS-MCSCF and SOCI IPs.

IV. THE NATURE OF LOW-LYING ELECTRONIC STATES OF TlH_n, InH_n, AND THEIR IONS

A. SOCI wave functions

The leading configurations of the $^2A_1$ states of InH_2 and TlH_2 are $1a_1^2 1b_2^2 2a_1^1$. The contributions of the leading configuration to the $^2A_1$ state are 94% and 93%, respectively, for InH_2 and TlH_2. The $1a_1$ orbital was found to be $M(ns) + M(np_z) + H_1(1s) + H_2(1s)$ wherein the metal *ns* orbital makes the predominant contribution to the $1a_1$ orbital. The $2a_1$ orbital has a much greater np_z character and comparable $H_1(1s) + H_2(1s)$ character. The $1b_2$ orbital is composed on $M(np_y) + H_1(1s) - H_2(1s)$. Consequently, both the $1b_2$ and $1a_1$ orbitals are strongly bonding while the $2a_1$ orbital is relatively less bonding.

The $^2B_1$ states of both InH_2 and TlH_2 exhibit an interesting behavior as a function of θ. Near the saddle point the $^2B_1$ state was found to be a nearly equal mixture of the $1a_1^2 2a_1^2 1b_1$ and $1a_1^2 1b_2^2 1b_1$ configurations. At larger bond angles the latter configuration dominates so that the $^2B_1$ state becomes $1\sigma_g^2 1\sigma_u^2 1\pi_u$ in the linear limit. Consequently, the barrier in the $^2B_1$ state arises from this avoided crossing. The sharp barrier in the $^2A_1$ state is due to superposition of two types of surfaces, one arising from $M(^2P) + H_2$ and the other form the molecular-like MH_2 surface.

The leading configuration of the $^1\Sigma_g^+$ states of both InH_2^+ and TlH_2^+ are the same ($1\sigma_g^2 1\sigma_u^2$). Note that the removed electron upon ionization comes from the highest occupied a_1 orbital of MH_2. The weight of the leading configuration in the SOCI wave functions is 93% and 94%, for InH_2^+ and TlH_2^+, respectively.

The ground states of InH_3 and TlH_3 are well described by the $1a_1'^2 1e'^4$ configuration in the D_{3h} group. Therefore, removal of an electron from the $1e'$ orbital results in a $^2E'$ state arising from the $1a_1'^2 1e'^3$ configuration. This state undergoes a Jahn–Teller distortion to yield $^2B_2(C_{2v})$ and $^2A_1(C_{2v})$ components in the C_{2v} symmetry. The $^2B_2$ state of the ion is found to be lower in energy. The leading configuration ($1a_1^2 2a_1^2 1b_2$) of the $^2B_2$ state of TlH_3^+ makes only 90% contribution. The second configuration, $1a_1^2 2a_1 3a_1 1b_2$ makes 4% contribution in the CASSCF. Evidently

MCSCF/MRCI treatment is warranted to represent the Jahn–Teller states of TiH_3^+ and InH_3^+.

B. RCI compositions

Table VII shows the RCI compositions as obtained from the weights of the RCI wave function. First we note that spin–orbit mixing of different states for InH_2 add up to only 0.27%. Hence we conclude that spin–orbit contaminations are relatively much smaller.

The spin–orbit contamination of the lowest E state of TlH_2 is significant as seen from Table VII. Especially, the $^2B_1$ state of TlH_2 makes a significant contribution of 2% even near the θ_e of the $^2A_1$ state. As seen from Fig. 1, these states come closer as θ increases becoming degenerate at $\theta = 180°$. At $\theta = 180°$, the merging of the two states results in $^2\Pi_u(1/2_u)$ and $^2\Pi_u(3/2_u)$ components.

The spin–orbit mixing is somewhat smaller for the closed shell $^1A_1'(D_{3h})$ state primarily because there are no low-lying excited states which yield A_1' symmetry in the D_{3h}^2 group.

The spin–orbit contamination of the two Jahn–Teller components of TlH_3^+ is non-negligible even at the equilibrium geometry of the $^2B_2$ state of TlH_3^+. The spin–orbit contaminations by the $^4A_1$ and $^4B_2$ states of TlH_3^+ are also non-negligible.

The spin–orbit contamination of the $^1\Sigma_{0^+}^+$ and $^3\Pi_{0^+}$ states is also significant in the diatomic TlH. The $^3\Pi_{0^+}$ contribution adds up to 1.8%. Consequently, even near the potential wells of TlH_n, spin–orbit effects cannot be neglected. In the dissociation limit, as noted already, spin–orbit effects are very substantial. Consequently, for computing bond dissociation energies spin–orbit coupling must be included.

C. Mulliken populations

Table VIII shows the Mulliken populations of some states of MH_2, MH_2^+, MH_3, and MH_3^+, species. It is evident from Table VIII that there is considerable sp^2 hybridization in MH_2 and MH_3 species near their equilibrium geometries. For example, the $^2A_1$ and $^1A_1'$ state of InH_2 and InH_3 have considerably smaller s populations and larger p populations. For TlH_n the $6s$ population is larger primarily due to the relativistic mass–velocity stabilization of the outer $6s^2$ shell.

A critical comparison of the population of InH_2 and InH_2^+ reveal that 58% of the removed electron comes from the In($5p$) orbital in the ionization process. Most of the remaining part (32%) of the ionization takes place on H.

The TlH_2 molecule upon ionization loses 54% of its electronic density from the $6p$ orbital while the H atom sheds 34% of the electronic density. Thus the loss of electronic density from the hydrogen atoms is comparable in both TlH_2 and InH_2 upon ionization.

The total M–H overlaps in InH_2 (1.29) are larger than the corresponding overlaps in TlH_2 (1.084). This trend is consistent with the significantly weaker bonding in TlH_2 compared to InH_2. The corresponding total Ga–H overlaps in GaH_2 is 1.36. Therefore Tl–H bonding is significantly weakened compared to GaH_2 and InH_2.

The M–H overlaps in MH_2^+ are larger than the corresponding overlaps of the neutral species while the total M–H overlaps of MH_3^+ (1.68 for TlH_3^+) are smaller than the sum of the three overlaps of the neutral MH_3 (2.37). This trend is consistent with the shorter M–H bonds upon ionization in MH_2 while two of the bonds are weakened upon ionization of MH_3.

TABLE VIII. Mulliken population analysis of MH_2, MH_2^+, MH_3, and MH_3^+ (M = In, Tl).

Molecule	State	M(s)	M(p)	M–H Overlap per bond
InH_2	$^2A_1$	1.36	1.359	0.64
	$^2\Pi_u$	1.24	1.699	0.68
	$^4\Pi_u$	1.24	1.698	0.68
InH_2^+	$^1\Sigma_g^+$	1.37	0.783	0.68
	$^1\Pi_g$	1.2	1.179	0.37
	$^1\Pi_u$	0.83	1.479	0.36
TlH_2	$^2A_1$	1.5	1.243	0.54
	$^2\Pi_u$	1.4	1.644	0.64
TlH_2^+	$^1\Sigma_g^+$	1.55	0.701	0.61
TlH_3	$^1A_1'$	1.43	1.45	0.79
TlH_3^+	$^2B_2$	1.4	0.86	0.7,[a] 0.49[b]
InH_3	$^1A_1'$	1.2	1.45	0.73
InH_3^+	$^2B_2$	1.27	0.96	0.65,[a] 0.46[b]

[a] Unique M–H bond overlap.
[b] MH overlap per bond for the two equivalent M–H bonds.

V. CLUSTER-SIZE DEPENDENCE OF IPs AND BOND ENERGIES

A. Bond energies

Figure 6 shows the plots of $D_e(H_{n-1}Tl\text{–}H)$ and $D_e(H_{n-1}In\text{–}H)$ for $n = 1$–3. These trends for both TlH_n and InH_n reveal that TlH_3 and InH_3 are the most stable of all three hydride clusters. This is consistent with trivalent nature of the group (III) elements. It is remarkable to note that the D_e falls down significantly upon addition of a hydrogen atom to InH or TlH but rises beyond the D_e of the monomer (diatomic) as one more H atom is added to yield InH_3 or TlH_3. This trend is consistent with the closed shell $^1\Sigma^+$ and $^1A_1'(D_{3h})$ ground states of TlH(InH) and $TlH_3(InH_3)$, respectively.

The D_es of MH_3^+ (M = In,Tl) show an inverted trend,

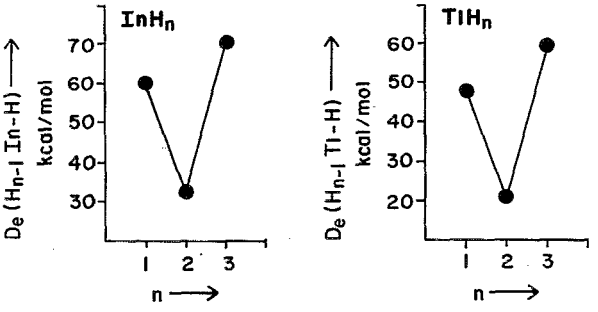

FIG. 6. Bond energies of TlH_n and InH_n ($n = 1$–3).

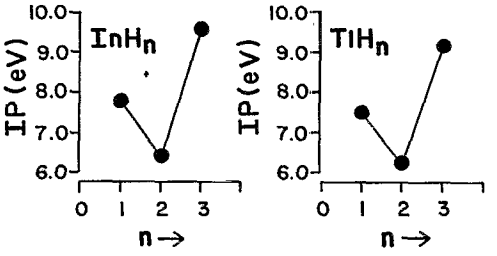

FIG. 7. Adiabatic IPs of TlH_n and InH_n ($n = 1$–3).

i.e., peak at InH_2^+, TlH_2^+ and low values for InH^+ and InH_3^+. In fact as noted before the $D_e(TlH^+)$ is very small while TlH_3^+ is unstable relative to $TlH_2^+ + H$. This is because the closed shell ground states are destroyed upon ionization of InH(TlH) and $InH_3(TlH_3)$ while ionization of the dimer (InH_2, TlH_2) yields a closed shell ground state for the ion.

B. Adiabatic IPs

Figure 7 shows a plot of the adiabatic IPs of InH_n and TlH_n as a function of n. As seen from Fig. 7, the IPs of InH_n and TlH_n exhibit odd–even alternation as a function of n. That is the odd hydride clusters (InH, InH_3) have considerably larger IPs than the IPs of InH_2 and TlH_2. This again is consistent with the destruction of the closed shell ground states for the odd clusters while InH_2 and TlH_2 form stable closed shell ground states ($^1\Sigma_g^+$) upon ionization. Consequently, the dimers (InH_2, TlH_2) have smaller IPs compared to the odd clusters. The trend in the adiabatic IP is similar to the corresponding trend of D_es as seen by a comparison of Figs. 6 and 7.

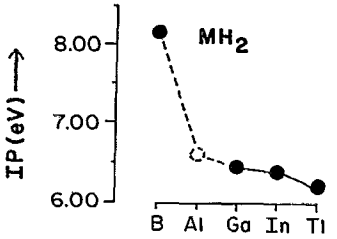

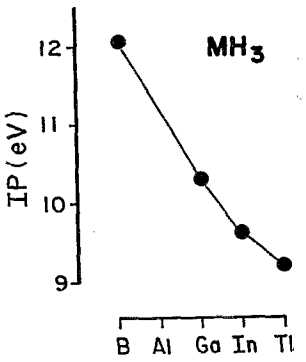

FIG. 8. Periodic trend in the IPs of BH_2–TlH_2 and period trend in the IPs of BH_3–TlH_3.

VI. PERIODIC TREND IN THE PROPERTIES OF BH_n–TlH_n (n=1–3)

Figure 8 shows the IPs of BH_2–TlH_2. The IP and D_e of BH_2 are from the calculation of Curtiss and Pople[11] while the GaH_2 values are from Ref. 21. As seen from Fig. 8, the IP of BH_2 is exceptionally high for this group. This is usually the case with the second row elements compared to other rows. The IPs of GaH_2 and InH_2 differ little. We expect the IP of AlH_2 to be close to GaH_2. Hence TlH_2 noticeably deviates from an expected collinear line joining AlH_2–InH_2. This deviation is mainly due to relativistic effects. The spin–orbit effect also stabilizes the open shell TlH_2 slightly more than the closed shell TlH_2^+ and thus the IP of TlH_2 is lower than InH_2.

Figure 8 also shows the periodic trend in the IPs of BH_3–TlH_3. While the IP of BH_3 is 12.03 eV,[11] the adiabatic IP of GaH_3 is only 10.32 eV.[21] Hence the IP of BH_3 is noticeably larger. We expect AlH_3, GaH_3, and InH_3 to form a collinear curve. TlH_3 has a lower IP compared to InH_3 akin to the InH_2–TlH_2 trend mainly due to relativistic effects.

Figure 9 shows the periodic trend in the bond energies of BH_2–InH_2 as well as BH_3–TlH_3. As seen from Fig. 9, BH_2 has considerably larger D_e(HB–H) (Ref. 11) compared to other members of the group. The D_e monotonically declines as one goes down the periodic table. The lower stability of TlH_2 and TlH_3 compared to other lighter analogs of Group III hydrides is explained based on relativistic effects.

Figure 10 shows an interesting geometry trends of BH_2–TlH_2 as well as BH_3–TlH_3. The plot of r_e(M–H) shows that the bond length noticeably contracts for TlH_3. This is mainly attributed to the enhanced ionicity of the Tl–H bonds compared to the In–H bonds. Note that TlH has a substantially larger dipole moment compared to InH.

As seen from Fig. 10, the θ_e (H–M–H) plot for BH_2–TlH_2 clearly reveals anomalies for BH_2 and TlH_2. The anomaly of BH_2 is understandable in view of greater sp^2 and s^2p^2 mixing for BH_3 and because BH_3 stands out as an exception in the group with regards to other properties (IP, D_e, etc.). The bond angle increase in TlH_2 compared to GaH_2 and InH_2 is mainly brought about by the spin–orbit coupling. In the case of TlH_2, the lowest $^2A_1$ state mixes with the low-lying $^2B_1$ state through spin–orbit coupling. Since the $^2B_1$ state forms a linear minimum, the spin–orbit contamina-

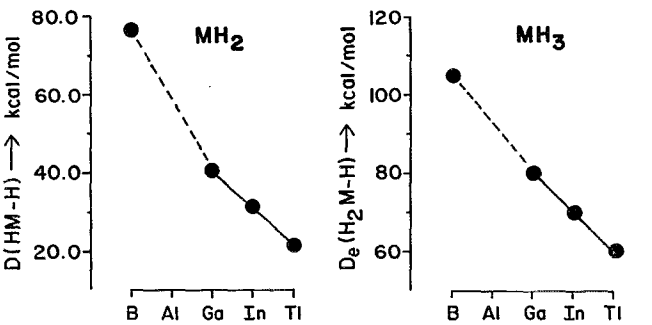

FIG. 9. Periodic trend in the bond energies of BH_3–TlH_3 and BH_2–TlH_2.

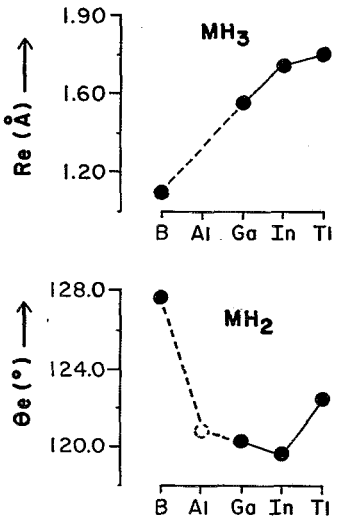

FIG. 10. Periodic trend in the equilibrium bond distances (M–H) of BH_3–TlH_3 and bond angles of BH_2–TlH_2. Note the increase in the bond angle of TlH_2 which is brought about by spin–orbit coupling.

tion of $^2A_1$ with $^2B_1$ increases the θ_e of the $^2A_1$ state. Therefore, clearly spin–orbit effects play an interesting role in the geometry of TlH_2.

VII. CONCLUSION

In this investigation we studied potential energy surfaces of TlH_2, InH_2, TlH_2^+, and InH_2^+ and the ground states of TlH_3, InH_3, TlH_3^+, and InH_3^+. The ground states of MH_2 neutral molecules were found to be bent ($\theta_e \sim 120°$) while the ground states of MH_2^+ were found to be linear $^1\Sigma_g^+$ states. The ground states of MH_3 molecules were found to be $^1A_1'(D_{3h})$ with planar–triangular geometries while the ground states of MH_3^+ positive ions are found to be Jahn–Teller distorted $^2B_2$ states with C_{2v} geometries. The TlH^+ ion is found to be only less than a kcal/mole bound while InH^+ ion is more strongly bound. A comparison of the adiabatic IPs and stepwise bond energies of all MH_n and TlH_n reveal odd–even alternation as a function of n. The properties of TlH_n were found to be altered to a significant extent due to relativistic effects. The spin–orbit coupling increases the θ_e of the ground state of TlH_2 by almost 1°. Our calculated D_e of TlH is in excellent agreement with the experimental value.

ACKNOWLEDGMENT

This research was supported by the National Science Foundation through Grant No. CHE88-18869.

[1]Y. S. Lee, W. C. Ermler, and K. S. Pitzer, J. Chem. Phys. **73**, 360 (1980).
[2]P. Pyykkö and J. P. Desclaux, Chem. Phys. Lett. **42**, 545 (1976).
[3]P. A. Christiansen and K. S. Pitzer, J. Chem. Phys. **73**, 5160 (1980).
[4]J. G. Snijders and P. Pyykkö, Chem. Phys. Lett. **75**, 5 (1980).
[5]N. C. Pyper, Mol. Phys. **42**, 1059 (1981).
[6]P. A. Christiansen and K. S. Pitzer, J. Chem. Phys. **74**, 1162 (1981).
[7]K. S. Pitzer and P. A. Christiansen, Chem. Phys. Lett. **77**, 589 (1981).
[8]K. S. Pitzer, Acc. Chem. Res. **12**, 271 (1979).
[9]P. A. Christiansen, K. Balasubramanian, and K. S. Pitzer, J. Chem. Phys. **76**, 5087 (1982).
[10]P. Schwedtfeger, Phys. Scripta **36**, 453 (1987).
[11]L. A. Curtiss and J. A. Pople, J. Chem. Phys. **90**, 2522 (1989); L. A. Curtiss and J. A. Pople, *ibid.* **89**, 614 (1988).
[12]R. C. Binning and L. A. Curtiss, J. Chem. Phys. **90**, 1860 (1990); R. C. Binning and L. A Curtiss, *ibid.* **92**, 3688 (1990).
[13]P. Rosmus and W. Meyer, J. Chem. Phys. **66**, 13 (1977).
[14]M. Page, G. F. Adams, J. S. Binkley, and C. F. Melius, J. Phys. Chem. **89**, 2198 (1985).
[15]J. Mauricio, O. Matos, P. A. Malmqvist, and B. Roos, J. Chem. Phys. **86**, 5032 (1987).
[16]T. P. Fehlner and W. S. Koski, J. Am. Chem. Soc. **86**, 2733 (1966).
[17]B. Ruscić, C. A. Mayhew, and J. Berkowitz, J. Chem. Phys. **88**, 5580 (1988).
[18]K. Balasubramanian and A. D. McLean, J. Chem. Phys. **85**, 5117 (1986).
[19]D. Dai and K. Balasubramanian, J. Chem. Phys. **93**, 1837 (1990).
[20]D. A. Chapman, J. Q. Li, K. Balasubramanian, and S. H. Lin, J. Chem. Phys. **88**, 3826 (1988).
[21]K. Balasubramanian, Chem. Phys. Lett. **164**, 231 (1989).
[22]G. B. Kim and K. Balasubramanian, J. Mol. Spectrosc. **134**, 412 (1989).
[23]J. Berkowitz, J. Chem. Phys. **89**, 7605 (1988); B. Ruscić, M. Schwarz, and J. Berkowitz, J. Chem. Phys. **92**, 1865 (1990).
[24]J. Berkowitz and H. Cho, J. Chem. Phys. **90**, 1 (1989).
[25]T. Ibuki, A. Hiraya, K. Shobatake, Y. Matsumi and M. Kawasaki, Chem. Phys. Lett. **160**, 152 (1989).
[26]J. Berkowitz, Account Chem. Res. **22**, 413 (1989).
[27]M. Colvin, R. S. Grev, H. F. Schaefer III, and J. Bicerano, Chem. Phys. Lett. **99**, 399 (1983).
[28]J. C. Rice and N. C. Handy, Chem. Phys. Lett. **107**, 365 (1984).
[29]K. Balasubramanian and M. Z. Liao, J. Phys. Chem. **92**, 4595 (1988).
[30]J. Berkowitz, J. P. Greene, H. Cho, and B. Ruscić, J. Chem. Phys. **86**, 1235 (1987).
[31]L. A. Curtiss and J. A. Pople, Chem. Phys. Lett. **144**, 38 (1988).
[32]L. G. M. Pettersson and P. E. M. Siegbahn, Chem. Phys. **105**, 355 (1986).
[33]K. Balasubramanian, J. Chem. Phys. **89**, 5731 (1988).
[34]R. A. Philips, R. J. Buenker, R. Beardsworth, P. R. Bunker, P. Jensen, and W. P. Kraemer, Chem. Phys. Lett. **118**, 60 (1985).
[35]K. K. Das and K. Balasubramanian, J. Chem. Phys. **93**, 5883 (1990).
[36]K. Balasubramanian, J. Chem. Phys. **91**, 2443 (1989).
[37]R. B. Ross, J. M. Powers, T. Atashroo, W. C. Ermler, L. A. LaJohn, and P. A. Christiansen, J. Chem. Phys. **93**, 6654 (1990).
[38]L. A. LaJohn, P. A. Christiansen, R. B. Ross, T. Atashroo, and W. C. Ermler, J. Chem. Phys. **87**, 2812 (1987).
[39]F. B. van Duijneveldt, IBM Research Report (1971).
[40]R. M. Pitzer, ARGOS integral codes.
[41]R. M. Pitzer and N. Winter, J. Phys. Chem. **92**, 3061 (1988).
[42]K. Balasubramanian, Chem. Phys. Lett. **127**, 585 (1986).
[43]C. E. Moore, *Tables of Atomic Energy Levels* (National Bureau of Standards, Washington, DC, 1971).
[44]The major authors of ALCHEMY II codes are B. Liu, B. Lengsfield, and M. Yoshimine.
[45]A. Bahnmaier, R. Urban, and H. Jones, Chem. Phys. Lett. **155**, 269 (1989).
[46]K. P. Huber and G. Herzbert, *Constants of Diatomic Molecules* (Van Nostrand, New York, 1979).
[47]Y. S. Lee and A. D. McLean, J. Chem. Phys. **76**, 735 (1982).